Chapter 8
PELDOR in Photo- and Radiation Chemistry

Abstract Early applications of PELDOR or DEER spectroscopy involved photochemistry and radiation chemistry. The atoms and molecules that absorbed the initial radiation; the radical pairs and/or excited states produced in that primary interaction of radiation with matter; and the subsequent chemical reactions are all long-standing issues that could be addressed by accurate measurements of pair distribution functions between the free radical products. The same issues arise in biological photosynthesis. The movement of electrons and holes during the entire sequence of reactions provided a clear picture of the sequence of reactions. Some of the initial applications of pulsed EPR methods, in particular ESE, to molecular systems focused on radiation chemistry and photochemistry (Salikhov et al in Electron spin echo and its applications. Nauka, Novosibirsk, 1976 [1]; Salikhov and Tsvetkov et al in Time domain electron spin resonance. John Wiley, New York, 1979 [2]; Bowman et al in Applications of EPR in radiation research. Springer, Heidelberg, pp 581–627, 2014 [3]). PELDOR emerged as a method focusing on the spatial distributions of products.

8.1 Radical Pairs Formed by Photolysis

8.1.1 Hydroquinone in Sulfuric Acid

Many important physicochemical processes form paramagnetic centers in pairs. For instance, the ultraviolet, or UV, photolysis of solids often produces an electron which becomes trapped by acceptors or the medium after travelling some distance. The holes resulting from loss of these electrons undergo analogous motion and trapping. Reactions of products with each other also occur. The distance between the pairs of paramagnetic products is described by a distance distribution function $F(r)$ and can be studied by PELDOR. If $F(r)$ is rather broad, the PELDOR signal has no visible oscillations. Nevertheless, information on the distribution of radical pairs can be obtained from analysis of the PELDOR time trace.

Y. D. Tsvetkov et al., *Pulsed Electron–Electron Double Resonance*,
https://doi.org/10.1007/978-3-030-05372-7_8

The pioneering PELDOR study [4] investigated radical pairs, composed of a hydrogen atom and a hydroquinone radical, trapped in frozen 8 M aqueous H_2SO_4 or D_2SO_4 glasses containing dissolved hydroquinone. The paramagnetic centers are formed by photoionization of the hydroquinone $Ar(OH)_2$ by UV light at 77 K:

$$\begin{gathered} Ar(OH)_2 \xrightarrow{UV} Ar(OH)_2^{\cdot +} + e^{\cdot -} \\ e^{\cdot -} + H_3O^+ \rightarrow H^{\cdot} + H_2O \\ \hline Ar(OH)_2 + H_3O^+ \xrightarrow{UV} Ar(OH)_2^{\cdot +} + H^{\cdot} + H_2O \end{gathered}$$

The observed distance distribution is governed by two factors: (1) the free path length of an electron prior to trapping by H_3O^+; and (2) the diffusion path length of hydrogen atoms before trapping in the matrix. In the PELDOR experiments, the hydrogen atoms were the A spins and produced the spin echo signals. The pump pulse was applied at the EPR frequency of the hydroquinone radical ions $Ar(OH)_2^{\cdot +}$, which were the B spins, Fig. 8.1a. The PELDOR time trace $V(T)$ from the hydrogen atoms depends on the concentration of hydroquinone radical ions. This means that each hydrogen atom has dipolar interactions not just with its partner, or geminate, hydroquinone radical, but also with other hydroquinone radicals.

The PELDOR time trace can be separated into $V(T) = V_{INTER}V_{INTRA}$ because the hydroquinone radicals are distributed uniformly throughout the matrix, Eq. 1.13. The V_{INTRA} was determined from the dependence of $V(T)$ on the concentration of hydroquinone radicals, and was then used to determine $F(r)$, approximating $\Phi(T)$, Eq. 1.11, in those early days of PELDOR, as a step function. The PELDOR data gave a distribution function with a maximum at 4.5 nm, Fig. 8.1. Integration of $F(r)$ reveals that 63% of the radicals are within 8.5 nm of their geminate radical partner and nearly all are within 10 nm. The actual shape of $F(r)$ is difficult to determine at the longer distances because the distant radical pairs have little impact on $V(T)$.

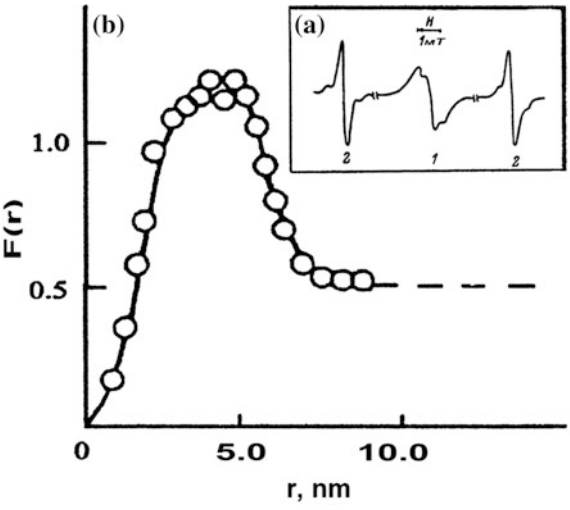

Fig. 8.1 UV-irradiated, frozen hydroquinone solutions in 8 M H_2SO_4, **a** EPR spectrum of paramagnetic centers formed in this system: *1* hydroquinone radicals, B spins and *2* hydrogen atoms, A spins; **b** the $F(r)$ function calculated from the PELDOR data. Reprinted from Milov et al. [4]

8.1.2 Aromatic Molecules in Hydrocarbons

The UV photolysis of aromatic compounds in hydrocarbon solutions at 77 K produces trapped solvent radicals. The mechanism for their formation involves absorption of two photons by an aromatic molecule with subsequent transfer of energy or charge to a nearby hydrocarbon solvent molecule followed by radical decomposition [5].

UV photolysis of naphthalene in glassy decalin at 77 K by light with $\lambda >$ 290 nm produces radicals whose EPR spectrum consists of six non-equidistant lines [6]. This spectrum belongs to radicals formed by abstraction of a hydrogen atom from a decalin molecule. The PELDOR time trace $V(T)$, at low concentrations of decalin radicals, reaches a limiting value V_p rather quickly, by $T \sim 100$ ns. Such behavior is characteristic of radicals distributed in clusters. The $V(T)$ of nitroxyl biradicals **3-9** and **3-10** have the same shape.

The PELDOR measurements used a bimodal resonator Sect. 2.5 whose modes were independently tuned to different lines of the decalin radical for ω_A and ω_B. This simplified the study of the V_p dependence on p_B. Changing the B_0 value moved the EPR spectrum relative to the pump and observe frequencies while the pulse amplitudes and durations remained constant. The V_p is a linear function of p_B with a slope that is independent of radical concentration or the extent of photolysis, Fig. 8.2. The relation $V_p \approx 1 - (N-1)p_B$, Eq. 1.26, was first derived for analysis

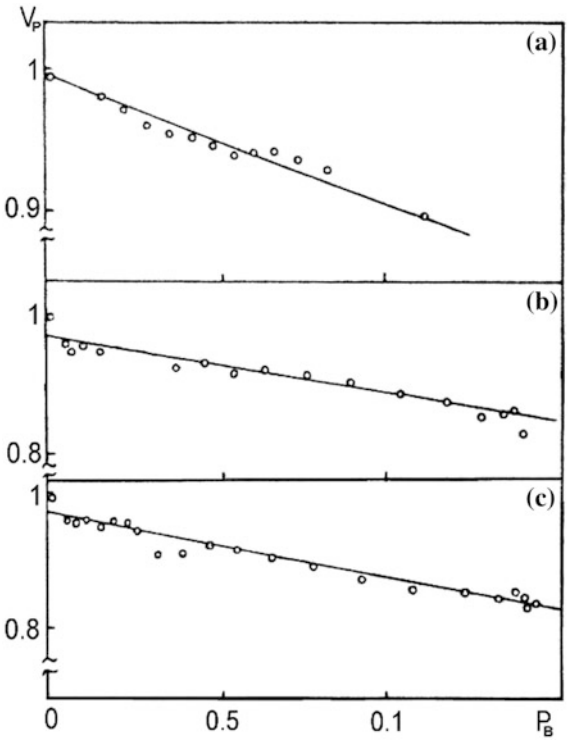

Fig. 8.2 Plots of the limiting V_p values versus p_B: **a** biradical **3.9**, **b** decalin radicals at 5.6×10^{17} cm^{-3} and **c** decalin radicals at 3×10^{17} cm^{-3}. Reprinted from Milov et al. [6] with permission of Elsevier B.V., copyright 1984

of this data [6]. The slope of the experimental straight line gave the number of radicals per cluster as $N = 1.85 \pm 0.2$. Thus, sensitized low-temperature photolysis of decalin produces stabilized, decalin radicals pairs. A limiting distance of 2.5 nm between radicals in the pair was estimated.

8.2 Radical Pairs in Photosynthetic Systems

Photosynthesis is one of the most important physicochemical processes. It converts solar light energy into electrochemical energy and is the basis for life on earth. The photosynthetic reactions involve energy, electron and proton transfers, with radical ions and free radicals as direct participants or by-products. Information on distances between these paramagnetic centers and their mutual orientation is of considerable importance in photosynthesis research since it provides a critical connection between structure and function. The vast majority of photosynthetic studies by PELDOR were carried out on Photosystem II (PSII) of green plants. The structural context for the photosynthetic reactions was known from X-ray diffraction studies [7] and a general outline of the reactions was known from extensive biophysical and spectroscopic studies. But the choreography of the movement of electrons, protons, molecules and proteins, as energy was captured and stored, was sometimes the focus of intense speculation. The overall scheme in PSII is roughly sketched below:

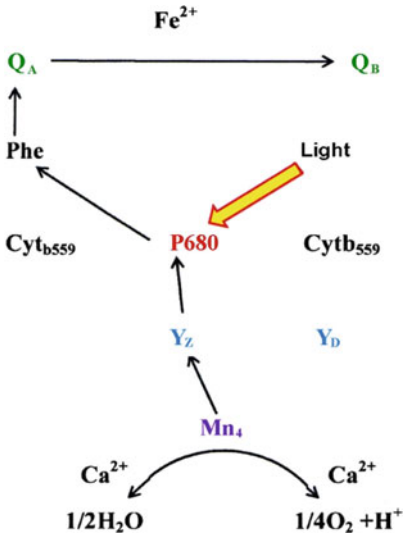

At the center of PSII is the primary electron donor P680, a chlorophyll *a* dimer with a distinctive optical absorption maximum at 680 nm. Light is absorbed by antenna pigments that funnel the excitation energy to P680, initiating a series of electron

transfers in PSII. An electron from the excited P680 is relayed, *via* an intermediate acceptor pheophytin Phe, to the primary electron acceptor, quinone Q_A, and later on to the secondary acceptor, quinone Q_B. The electron vacancy or hole on P680 is rapidly filled by a sequence of redox reactions involving tyrosine radicals Y_Z and Y_D, and a cluster of manganese ions Mn_4. The Mn_4 carries out the crucial steps of water splitting and formation of oxygen. Each electron can be followed through the series of transient paramagnetic centers detected by EPR spectroscopy. These centers, along with systems that model various properties of the reaction center of PSII, has been studied extensively by magnetic resonance [8, 9].

8.2.1 Stable Radical Pairs

PELDOR and other pulsed dipolar methods were applied to several relatively-stable radical pairs in PSII. At room temperature, the oxidized $Y_Z^{\cdot +}$ has a short lifetime and can barely be detected by EPR spectroscopy. However, oxidized $Y_D^{\cdot +}$ is stable in the dark and is readily detected. The EPR spectrum of $Y_D^{\cdot +}$ is a single, narrow line with $g \approx 2$. The Mn_4 cluster has five states (S_0–S_4); each state has a different EPR spectrum. In addition, removal of a calcium ion (Ca) from the Mn_4 cluster leaves it redox active but unable to release oxygen. A review of stable paramagnetic centers in PSII studied by PELDOR and other EPR methods can be found in [10].

The oxygen-evolving and the Ca-depleted PSII systems were studied [11]. The EPR spectra of the S_2 and S_3 states of Mn_4 are quite different from those of $Y_D^{\cdot +}$ which made it possible to measure the dipolar coupling between these species by PELDOR. The pump pulse was applied to $Y_D^{\cdot +}$ and the spin echo signal was produced from Mn_4 and shows clear modulation, Fig. 8.3. The distance between the unpaired electron spin in the S_2 state and $Y_D^{\cdot +}$ is $r = 2.7$ nm in oxygen-evolving and in Ca-depleted PSII, Table 8.1. The distance between the spins of the S_3 state of Ca-depleted PSII and $Y_D^{\cdot +}$ is slightly larger at 3.0 nm, and even longer for the S_o state of the Mn_4 cluster [11]. The distances between the $Y_D^{\cdot +}$ cation and the spin of Mn_4 are different because the spin of Mn_4 is localized on different ions of the cluster in its different S states.

PELDOR experiments with other stable radical pairs in PSII are difficult at X-band because their EPR spectra have strong overlap. It is often impossible to select ω_A and ω_B for selective mw excitation of individual centers. But X-band EPR experiments were possible between a number of centers, Table 8.1 [11–16].

The reaction centers of PSII are embedded in specific structures of the chloroplast membrane called thylakoids. The donor and acceptor regions of PSII are localized on opposite sides of the thylakoid membrane. Their orientation relative to the membrane surface was studied by the first PELDOR orientation measurements [17]. A Mylar sheet was coated with a layer of alligned PSII and the sheet was oriented

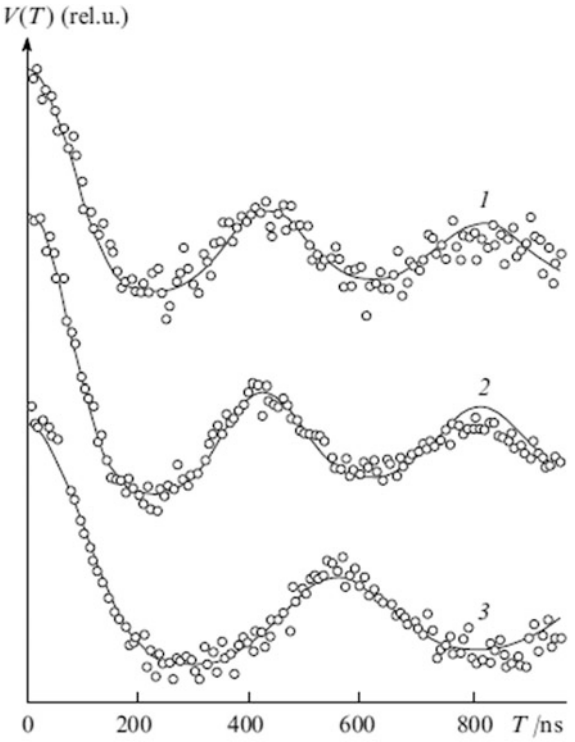

Fig. 8.3 The $V(T)$ of pairs of paramagnetic centers in PSII: *1* oxygen-producing PSII with active Mn_4 clusters in S_2; *2* Ca-depleted PSII with Mn_4 in S_2; and *3* Ca-depleted PSII with Mn_4 in S_3; *points* denote experimental data and *solid lines* denote calculations. Reproduced from Tsvetkov et al. [39]

Table 8.1 Distances between paramagnetic centers in PSII determined by PELDOR

Pair of centers	Distance, nm	Reference
Y_D—$Mn_4(S_2)$	2.71 ± 0.02	[11]
Y_D—$Mn_4(S_3)$	2.97 ± 0.02	[11]
Y_D—$Mn_4(S_0)$	3.40 ± 0.05	[12]
Q_A—Chl_Z	3.4 ± 0.1	[13]
Q_A—Y_Z	3.4 ± 0.05	[14]
Q_A—Y_Z	3.45 ± 0.1	[15]
Q_A—Cyt_{b559}	4.0 ± 0.1	[16]

relative to the external magnetic field B_0. PELDOR time traces of the radical pair consisting of $Y_D^{\cdot +}$ and the S_2 state of Mn_4 were measured. The vector connecting the two centers makes a 20 ±2° angle with the normal to the thylakoid membrane surface.

Radical pairs have also been produced by spin labeling proteins of the photosynthetic apparatus. This approach was used to study the protein component of light-harvesting complex LHCIIb, which contains chlorophylls *a* and *b* and is present in both PSI and PSII. Spin labels were introduced pairwise into the protein and the distance distribution $F(r)$ between pairs were determined [18]. The $F(r)$ for

all labels near the N-terminus of the protein appear to be bimodal, corresponding to two different conformations. The two conformers were assigned to LHCIIb in the two different photosystems, namely, PSI and PSII [18]. The N-terminal domain is involved in light flux regulation, suggesting a role for conformational changes.

8.2.2 *Transient Radical Pairs*

PELDOR studies on stable radical pairs in 8.2.1 were made at X-band. Higher EPR frequencies, where g-values can be resolved, provide additional opportunities to obtain the orientation of the donors, acceptors and cofactors in addition to distances. The most extensive high-frequency studies [19–21] focused on transient radical pairs of the reaction center (RC) of photosynthetic bacteria, Fig. 8.4.

A short-lived radical pair, $P_{865}^{\cdot+}Q_A^{\cdot-}$, Fig. 8.4, was produced by a laser pulse in frozen solutions of reaction centers from the photosynthetic bacteria *Rb. sphaeroides* and studied by W-band EPR spectroscopy at 95 GHz [19, 20]. Some of the reactions actually become faster at low temperature, so measurements were made near 150 K to reduce the radical pair lifetime. At W-band, the EPR spectra of these radical ions only partially overlap, which enables measurements at the g_{xx}, g_{yy}, g_{zz} of $Q_A^{\cdot-}$ and $P_{865}^{\cdot+}$ [22], so that their orientation within the pair as well as their

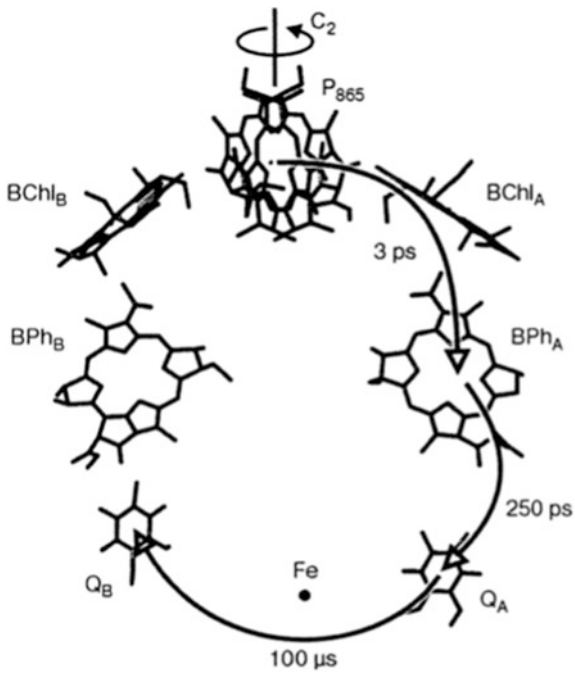

Fig. 8.4 X-ray structure of the cofactors in the reaction center of *Rhodobacter sphaeroides*; the cofactors P_{865} (bacteriochlorophyll *a* dimer), $BChl_A$ and $BChl_B$ (bacteriochlorophyll *a*), BPh_A and BPh_B (bacteriopheophytin *a*), Q_A and Q_B (ubiquinone-10), Fe (Fe^{2+} ion) are related by approximate C_2 symmetry of the RC proteins; yet, the light-induced electron transfer (ET) proceeds almost exclusively along the A branch; *Arrows* indicate the ET steps with their time constants. Reproduced from Schnegg et al. [20], with permission Springer-Verlag, copyright 2007

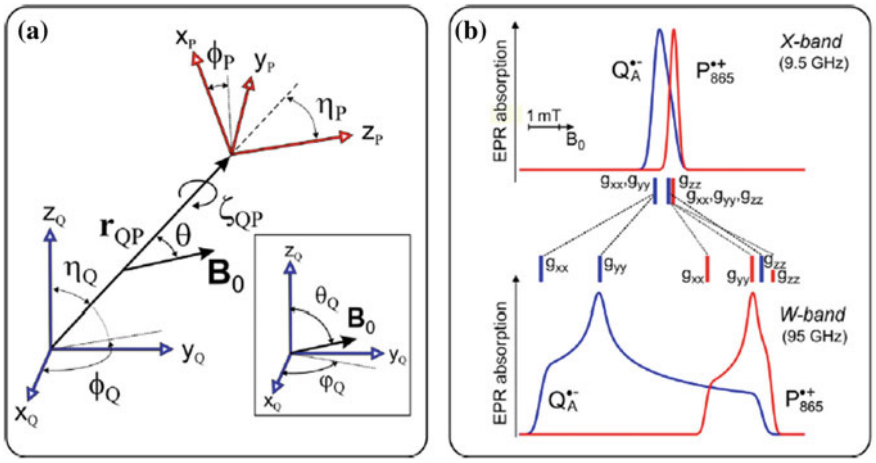

Fig. 8.5 **a** Geometry of the g-tensor frames $R_Q(x_Q, y_Q, z_Q)$ and $R_P(x_P, y_P, z_P)$ in terms of polar angles η_Q, ϕ_Q and η_P, ϕ_P and the dipolar vector r_{QP}; the angle ζ_{QP} is the relative tilt of the Q and P frames around the dipolar axis; **b** EPR absorption spectra of $P_{865}^{\cdot+}$ and $Q_A^{\cdot-}$ radicals at X-band (9.5 GHz) and W-band (95 GHz); the principal g-values of both radicals are indicated, with the maximum amplitude of each spectrum normalized. Reproduced from Schnegg et al. [20] with permission Springer Nature, copyright 2007

distance were determined. The orientation of g-axes within the radical pair is shown in Fig. 8.5.

The RC radical pair produced by light is born in the singlet state. Therefore, the EPR spectrum is spin-polarized and has adsorptive and emissive components from the spin-correlated radical pair (SCRP) mechanism [23–26] and somewhat different selection rules [27, 28].

Figure 8.6a shows the mw pulse scheme used for 4pPELDOR on pulsed laser-generated SCRPs. The frequency ω_A of the three observe $\pi/2$ pulses was adjusted to an EPR transition of the observed spins, either $P_{865}^{\cdot+}$ or $Q_A^{\cdot-}$. During the time period T, the mw π pump pulse at ω_B was applied to flip the partner spins. The ω_A and ω_B, Fig. 8.6a, correspond to the resonance conditions at constant field for the principal g-values in the normal field-swept EPR spectrum.

The observed spins dephase during the time τ between the first and second $\pi/2$ observe pulses, in part from the dipolar field of the partner radical. But here, the dipolar field is reversed during τ following the third observe pulse when the A spins are refocused into a spin echo. Reversing the dipolar field modulates the spin echo with the frequency of the dipolar interaction.

The SCRP state produces two different echo signals, an in-phase signal S_{-y} and an out-of-phase signal S_x [29]. Figure 8.6 shows a typical $V(T)$ slice for S_x. The complete set of slices, measured by stepping the mw frequency ω_B through the spectrum of the partner radical, contains modulation for the pump pulse at each position within the EPR spectrum of the partner radical. The PELDOR spectrum is

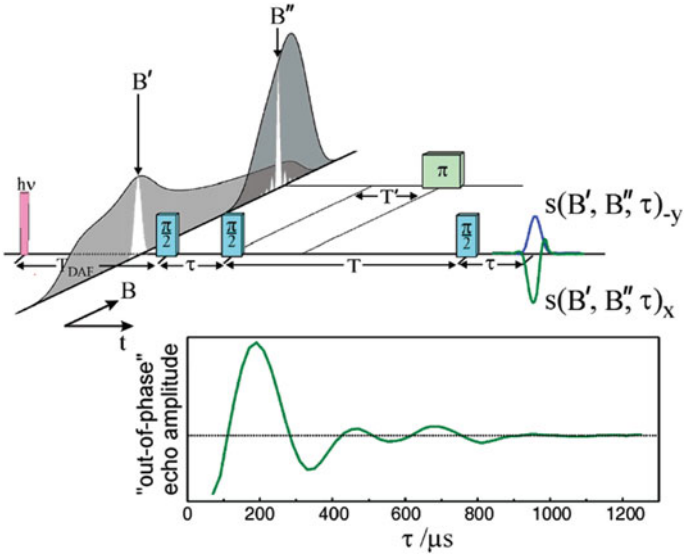

Fig. 8.6 *Upper:* Pulse sequence for the W-band PELDOR experiment on spin-correlated radical pairs generated by a laser flash in photosynthetic reaction centers: the thermally-equilibrated EPR spectra of both radicals, $P_{865}^{\cdot+}$ and $Q_A^{\cdot-}$, as well as the mw excitation bandwidths for typical mw pulse length settings are shown as a visual aid; *lower:* a representative example of a dipolar modulation echo-decay trace from the out-of-phase-detected echo versus τ is shown. Reproduced from Savitsky et al. [19] with permission American Chemical Society, copyright 2007

detected only for those $P_{865}^{\cdot+}$ or $Q_A^{\cdot-}$ radicals in a SCRP which are coupled by a dipolar interaction.

Information about the full 3D geometry of the radical pair, Fig. 8.5, is encoded in the modulation of these PELDOR spectra. Geometrical parameters for the $P_{865}^{\cdot+}Q_A^{\cdot-}$ radical pair were extracted by newly-developed methods [19, 20] and are compared to the ground-state $P_{865}^{\cdot+}Q_A^{\cdot-}$ radical pair, Table 8.2. No significant differences were seen, meaning that no substantial reorientation of P_{865} and Q_A occurs during the light-driven charge separation that produces the $P_{865}^{\cdot+}$ and $Q_A^{\cdot-}$ radical ion pair [7, 30].

Table 8.2 Angles and distances describing the geometry of the $P_{865}^{\cdot+}Q_A^{\cdot-}$ pair

P_{865} Q_A	η_Q^0	ϕ_Q^0	η_P^0	ϕ_P^0	ζ_{QP}^0	r, nm
Ground state pair[a]	97.4	246.2	66.2	79.5	49.5	2.84
PELDOR radical pair[b]	109.5	242	59	82	50	2.94

The angles are for the transition from the Q frame to the P frame, i.e., the dipolar vector direction is Q-P, Fig. 8.5a

[a]Reference pair: obtained from X-ray crystallographic data [19] of the dark state RC complemented by the W-band EPR single crystal investigation of $P_{865}^{\cdot+}$ [7]

[b]PELDOR radical pair: obtained from ESE-detected W-band EPR combined with PELDOR

The cofactor geometry in PSI was also studied by high-field PELDOR [31]. The short-lived ion-radical pair $P_{700}^{\cdot+}A_1^{\cdot-}$, where A_1 is phylloquinone, is analogous to $P_{865}^{\cdot+}Q_A^{\cdot-}$. The position and orientation of the reduced $A_1^{\cdot-}$ coincide with those of its parent A_1; again, no substantial orientation changes occur upon charge separation. On the other hand, several distinct orientations of the $P_{700}^{\cdot+}$ g-tensor axes were found and attributed to conformational substates of the $P_{700}^{\cdot+}$ radical ion with slightly different electron spin density distributions [31].

8.3 Spatial Distribution of Radicals from Radiolysis

The energy of hard radiation, e.g., α-, β- and γ-rays, and nuclear fission products, is deposited non-uniformly in liquids and solids, producing intermediates and reaction products, e.g., ions, electrons, atoms, and radicals, that are also spatially non-uniform. The regions containing products are known as tracks and spurs. These radical tracks and spurs were an early focus of pulse EPR and ESE in chemistry, e.g., see reviews [2, 3, 32].

Analysis of the PELDOR time trace $V(T)$ characterizes the number of spins in a group much better than classic spin echo methods. Even if there is a distribution in the number of spins in a group, PELDOR can give a weighted average or effective number of spins, Sects. 1.2.6 and 1.2.7. Consequently, one early application of PELDOR was to characterize the radical clusters in γ-irradiated cyclohexane, polyethylene and a number of organic acids [33–35].

Cyclohexyl radicals in crystalline cyclohexane, γ-irradiated at 77 K, produce a $V(T)$ similar to that of biradicals with a broad distance distribution [34]. There is an initial decay, in about 0.5 μs, to a limiting value V_p. The dependence of V_p on p_A and p_B was different from that of biradicals or radical pairs produced by sensitized photolysis, Sect. 8.1. The parameter N_{eff} depends on p_A, the probability or extent of excitation by observe pulses at ω_A for the cyclohexyl radicals while a biradical control **8-1** gave $N_{eff} = \sim 2.2$ independent of p_A, Fig. 8.7.

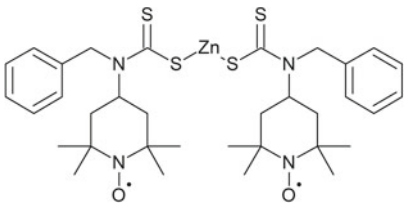

The dependence of N_{eff} on p_A in γ-irradiated cyclohexane is due to groups containing different numbers of radicals. Analysis of the change of V_p with p_A, Sects. 1.2.6, 1.2.7, and 1.5, gave some information about the number of radicals in

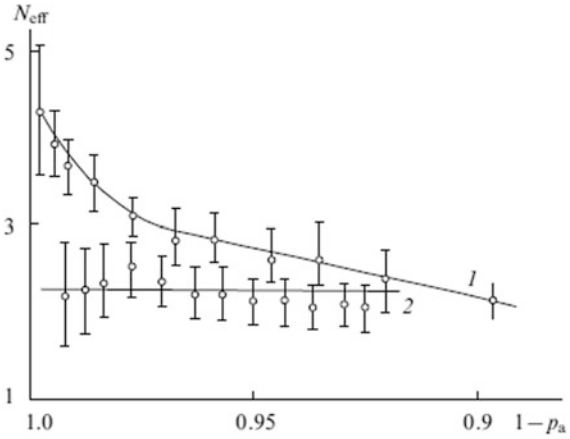

Fig. 8.7 Effective number of radicals, N_{eff}, versus excitation probability, p_A, by the observe pulses at ω_A: *1* for cyclohexyl radicals and *2* for nitroxyl biradicals **8-1**. Reproduced from Tsvetkov et al. [39]

a group. Most radicals, 75–90%, are distributed uniformly or in pairs, while the remaining 10–25% are in clusters containing three to several tens of radicals. The characteristic group size determined from the initial $V(T)$ is $r = \sim 2.5$ nm, which corresponds to a local radical density of $\sim 10^{20}$ cm^{-3}. High local concentrations like this are missed by two-pulse ESE because the dead time for ESE is greater than the short relaxation time at such radical densities. Thus, PELDOR gives much more detailed information about the spatial distribution of radicals in γ-irradiated systems than do ESE methods.

Alkyl radicals produced by γ-radiolysis of polyethylene and some organic acids gave similar results [35]. Irradiation and measurements were made at 77 K to minimize further radical reactions. Irradiated polyethylene, like irradiated cyclohexane, gave $V(T)$ that decay rapidly at short times, reaching a limiting value V_p, which depends on p_A and p_B. Careful analysis, Sect. 1.2.7, determined N_{eff} and the first and second moments of the distribution of number of radicals in groups [35]. Low-temperature radiolysis of polyethylene produces alkyl radicals in groups with an average of 2.4 radicals, second moment ≤ 6, and a radius of ≤ 2.5 nm.

PELDOR was used to probe the spatial distribution of radicals in DNA irradiated at 77 K to doses of 1.7–50 kGy by heavy-ion beams of 100 meV per nucleon ^{40}Ar ions having an LET of 300–400 keV/μm [36]. Such ions produce dense tracks of damage in their wake with extensive recombination of paramagnetic centers. At the doses used, the individual tracks are well separated and the samples had superimposable PELDOR spectra. The PELDOR time traces decayed smoothly over a range of p_B that varied by a factor of 12. At the smaller values of p_B, the signal intensity reached a limiting value that allowed determination of the number N of radicals contributing to the PELDOR time trace. The rate of decay to that limiting value gave the local concentration of those paramagnetic centers. The p_B was underestimated, slightly overestimating N and local concentration. This error is partly offset when the track radius is calculated. A global fit of all samples and data

gave $C_{loc} \sim 13.5 \times 10^{19}$ radicals cm^{-3} and a track radius of 6.8 nm, consistent with the LET and radiation chemical yield.

Polycrystalline ammonium tartrate was studied by PELDOR after γ-, neutron- and 19.3 meV proton-irradiation [37] following initial spin echo measurements of instantaneous diffusion. This is the first reported case of PELDOR $V(T)$ in irradiated materials with pronounced modulation not caused by nuclear modulation (ESEEM) artifacts [38]. The resolved modulation was attributed to radicals being trapped at multiples of the unit cell, but only along the crystal axes. The paper notes that this is the first report of radiation-generated radicals trapped preferentially only along the three crystallographic axes. Unfortunately, these remarkable $V(T)$ were not shown. The $F(r)$ extracted from the PELDOR data lies almost entirely between 2.0 and 5.5 nm with ripples at multiples of the unit cell dimension. This distribution was reproduced very closely by detailed simulations incorporating the crystal structure and anisotropic recombination. The observed and simulated differences in $F(r)$ with different types of radiation were suggested as providing a way to determine LET of unknown radiation by the ammonium tartrate dosimeter.

These brief examples show the promise of PELDOR for future investigations of the spatial properties of paramagnetic particles participating in elementary acts of photo- and radiation chemistry. The success with photoexcited photosynthetic systems emphasizes that PELDOR is applicable to transient excited states as well as stabilized radicals. Applications of PELDOR to functioning conductive polymers and photoconversion devices appear to be feasible.

References

1. Salikhov KM, Semenov AG, Tsvetkov YD (1976) Electron spin echo and its applications. Nauka, Novosibirsk
2. Salikhov KM, Tsvetkov YD (1979) Electron Spin echo studies of spin-spin interactions in solids. In: Kevan L, Schwartz RN (eds) Time domain electron spin resonance. John Wiley, New York, pp 231–278
3. Bowman MK, Maryasov AG, Tsvetkov YD (2014) EPR measurement of the spatial distribution of radiation damage. In: Lund A, Shiotani M (eds) Applications of EPR in radiation research. Springer, Heidelberg, pp 581–627. https://doi.org/10.1007/978-3-319-09216-4
4. Milov AD, Salikhov KM, Shirov MD (1981) Application of eldor in electron-spin echo for paramagnetic center space distribution in solids. Fiz Tverd Tela 23(4):975–982
5. Bagdasaryan KS (1976) Two-quantum photochemistry. Nauka, Moscow
6. Milov AD, Ponomarev AB, Tsvetkov YD (1984) Electron electron double-resonance in electron-spin echo—model biradical systems and the sensitized photolysis of decalin. Chem Phys Lett 110(1):67–72. https://doi.org/10.1016/0009-2614(84)80148-7
7. Klette R, Torring JT, Plato M, Mobius K, Bonigk B, Lubitz W (1993) Determination of the *g* tensor of the primary donor cation radical in single-crystals of *Rhodobacter sphaeroides* R-26 reaction centers by 3-mm high-field EPR. J Phys Chem-Us 97(9):2015–2020. https://doi.org/10.1021/j100111a047
8. Hoff AJ (ed) (1989) Advanced EPR: applications in biology and biochemistry. Elsevier, Amsterdam. https://doi.org/10.1016/b978-0-444-88050-5.50004-5

9. Kawamori A, Mino H, Hara H, Astashkin AV, Tsvetkov YD (1995) Multiple resonance in pulsed EPR with application to photosynthesis. Kwansei Gakuin Univ Annu Stud 64:221–231
10. Kawamori A (2003) Electron transfer and structure of plant photosystem II. In: Lund A, Shiotani M (eds) EPR of free radicals in solids: trends in methods and applications. Springer US, pp 529–563. https://doi.org/10.1007/978-1-4757-5166-6
11. Hara H, Kawamori A, Astashkin AV, Ono T (1996) The distances from tyrosine D to redox-active components on the donor side of Photosystem II determined by pulsed electron-electron double resonance. Bba-Bioenergetics 1276(2):140–146. https://doi.org/10.1016/0005-2728(96)00071-0
12. Kawamori A, Katsuta N, Arao S, Ishii A, Minagawa J, Mino H, Ono T (2001) Three-dimensional structure of photosystem II studied by pulsed EPR. In: Proceedings of 12th international congress on photosynthesis. CSIRO Publishing, Collingwood, Victoria
13. Kawamori A, Ono TA, Ishii A, Nakazawa S, Hara H, Tomo T, Minagawa J, Bittl R, Dzuba SA (2005) The functional sites of chlorophylls in D1 and D2 subunits of Photosystem II identified by pulsed EPR. Photosynth Res 84(1–3):187–192. https://doi.org/10.1007/s11120-005-1000-y
14. Kawamori A, Katsuta N, Hara H (2003) Structural analysis of three-spin systems of photosystem II by PELDOR. Appl Magn Reson 23(3–4):557–569. https://doi.org/10.1007/Bf03166641
15. Kawamori A, Katsuta N, Mino H, Ishii A, Minagawa J, Ono TA (2002) Positions of Q_A and Chl_Z relative to tyrosine Y_Z and Y_D in photosystem II studied by pulsed EPR. J Biol Phys 28 (3):413–426. https://doi.org/10.1023/A:1020312621949
16. Kuroiwa S, Tonaka M, Kawamori A, Akabori K (2000) The position of cytochrome b_{559} relative to Q_A in photosystem II studied by electron-electron double resonance (ELDOR). Biochim Biophys Acta 1460(2–3):330–337
17. Astashkin AV, Hara H, Kawamori A (1998) The pulsed electron-electron double resonance and "2+1" electron spin echo study of the oriented oxygen-evolving and Mn-depleted preparations of photosystem II. J Chem Phys 108(9):3805–3812. https://doi.org/10.1063/1.475770
18. Jeschke G, Bender A, Schweikardt T, Panek G, Decker H, Paulsen H (2005) Localization of the N-terminal domain in light-harvesting chlorophyll a/b protein by EPR measurements. J Biol Chem 280(19):18623–18630. https://doi.org/10.1074/jbc.M501171200
19. Savitsky A, Dubinskii AA, Flores M, Lubitz W, Mobius K (2007) Orientation-resolving pulsed electron dipolar high-field EPR spectroscopy on disordered solids: I. structure of spin-correlated radical pairs in bacterial photosynthetic reaction centers. J Phys Chem B 111 (22):6245–6262. https://doi.org/10.1021/jp070016c
20. Schnegg A, Dubinskii AA, Fuchs MR, Grishin YA, Kirilina EP, Lubitz W, Plato M, Savitsky A, Mobius K (2007) High-field EPR, ENDOR and ELDOR on bacterial photosynthetic reaction centers. Appl Magn Reson 31(1–2):59–98. https://doi.org/10.1007/Bf03166248
21. Mobius K, Lubitz W, Savitsky A (2013) High-field EPR on membrane proteins—Crossing the gap to NMR. Prog Nucl Mag Res Sp 75:1–49. https://doi.org/10.1016/j.pnmrs.2013.07.002
22. Fuchs MR, Schnegg A, Plato M, Schulz C, Muh F, Lubitz W, Mobius K (2003) The primary donor cation $P^{+\cdot}$ in photosynthetic reaction centers of site-directed mutants of *Rhodobacter sphaeroides*: g-tensor shifts revealed by high-field EPR at 360 GHz/12.8 T. Chem Phys 294 (3):371–384. https://doi.org/10.1016/s0301-0104(03)00319-7
23. Bowman MK, Budil DE, Closs GL, Kostka AG, Wraight CA, Norris JR (1981) Magnetic resonance spectroscopy of the primary state, P^F, of bacterial photosynthesis. P Natl Acad Sci USA 78(6):3305–3307
24. Norris JR, Bowman MK, Budil DE, Tang J, Wraight CA, Closs GL (1982) Magnetic characterization of the primary state of bacterial photosynthesis. Proc Natl Acad Sci U S A 79 (18):5532–5536

25. Closs GL, Forbes MDE, Norris JR (1987) Spin-polarized electron-paramagnetic resonance-spectra of radical pairs in micelles—observation of electron-spin spin interactions. J Phys Chem-Us 91(13):3592–3599. https://doi.org/10.1021/j100297a026
26. Stehlik D, vanderEst A, Kamlowski A (1996) Transient spin states in the primary processes of photosynthesis. Ber Bunsen Phys Chem 100 (12):2028–2035
27. Hasharoni K, Levanon H, Tang J, Bowman MK, Norris JR, Gust D, Moore TA, Moore AL (1990) Singlet photochemistry in model photosynthesis—identification of charge separated intermediates by fourier-transform and CW-EPR spectroscopies. J Am Chem Soc 112 (18):6477–6481. https://doi.org/10.1021/ja00174a004
28. Bowman MK, Chen HJ, Maryasov AG (2017) Pulsed EPR Signals from Triplets. Z Fur Phys Chem-Int J Res in Phys Chem Chem Phys 231(3):637–652. https://doi.org/10.1515/zpch-2016-0869
29. Schweiger A, Jeschke G (2001) Principles of pulse electron paramagnetic resonance. Oxford University Press, Oxford, UK, New York
30. Stowell MHB, McPhillips TM, Rees DC, Soltis SM, Abresch E, Feher G (1997) Light-induced structural changes in photosynthetic reaction center: Implications for mechanism of electron-proton transfer. Science 276(5313):812–816. https://doi.org/10.1126/science.276.5313.812
31. Savitsky A, Niklas J, Golbeck JH, Mobius K, Lubitz W (2013) Orientation resolving dipolar high-field EPR spectroscopy on disordered solids: II. Structure of spin-correlated radical pairs in photosystem I. J Phys Chem B 117 (38):11184–11199. https://doi.org/10.1021/jp401573z
32. Tsvetkov YD (1983) Study of spatial peculiarities of formation and reactions of radicals in a solid-phase by the electron-spin echo method. Usp Khim 52(9):1514–1537
33. Tsvetkov YD (1989) ELDOR in ESE study of magnetic dipole-dipole interactions. In: Keijzers CP, Reijerse EJ, Schmidt J (eds) Pulsed EPR: a new field of applications. North Holland, Amsterdam, pp 206–218
34. Ponomarev AB, Milov AD, Tsvetkov YD (1988) Double electron-electron resonance in electron-spin echo and the spatial distribution of radicals formed by irradiation of frozen cyclohexane. Khim Fiz 7(12):1673–1679
35. Ponomarev AB, Milov AD, Tsvetkov YD (1990) Double electron-electron resonance in electron-spin echo—spatial distribution of radicals forming during radiolysis of polyethylene, monocarboxylic and dicarboxylic-acids. Khim Fiz 9(4):498–503
36. Bowman MK, Becker D, Sevilla MD, Zimbrick JD (2005) Track structure in DNA irradiated with heavy ions. Radiat Res 163(4):447–454. https://doi.org/10.1667/rr3338
37. Marrale M, Brai M, Barbon A, Brustolon M (2009) Analysis of the spatial distribution of free radicals in ammonium tartrate by pulse EPR techniques. Radiat Res 171(3):349–359. https://doi.org/10.1667/Rr1358.1
38. Jeschke G (2012) DEER distance measurements on proteins. Annu Rev Phys Chem 63 (1):419–446. https://doi.org/10.1146/annurev-physchem-032511-143716
39. Tsvetkov YD, Milov AD, Maryasov AG (2008) Pulsed electron–electron double resonance (PELDOR) as EPR spectroscopy in nanometre range. Russ Chem Rev 77:487–520